Research Square

Preprints are preliminary reports that have not undergone peer review. They should not be considered conclusive, used to inform clinical practice, or referenced by the media as validated information.

Integrated Analysis of Gutenberg Richter b-value and Apparent Stress Reveals Spatial Heterogeneity of Seismotectonic Conditions in the Gulf of California Rift System

Ananta Saputra
Hasanuddin University
Muh. Farid Wajedy
muhfaridwajedy@unhas.ac.id

Hasanuddin University

Research Article

Keywords: Gulf of California Rift System, Gutenberg-Richter b-value, apparent stress, seismic hazard, seismotectonic heterogeneity

Posted Date: October 21st, 2026

DOI: https://doi.org/10.21203/rs.3.rs-11174777/v1

License: This work is licensed under a Creative Commons Attribution 4.0 International License. Read Full License

Additional Declarations: No competing interests reported.

Integrated Analysis of Gutenberg Richter b-value and Apparent Stress Reveals Spatial Heterogeneity of Seismotectonic Conditions in the Gulf of California Rift System

Ananta Saputra[1], Muh. Farid Wajedy[1*]

[1]Program Study of Geophysics, Department of Geophysics, Faculty of Mathematics and Natural Sciences, Hasanuddin University, Makassar, 90245, Indonesia.

e-mail: *muhfaridwajedy@unhas.ac.id*

Abstract

The Gulf of California Rift System is an active continental rift characterized by heterogeneous seismicity, requiring a comprehensive evaluation of regional seismotectonic conditions. This study aims to characterize the spatial heterogeneity of seismotectonic conditions by integrating the magnitude of completeness M_c, Gutenberg-Richter b-value, and apparent stress. Earthquake data from the United States Geological Survey (1900-2026) were declustered using the Gardner Knopoff algorithm, Mc was estimated using the Entire Magnitude Range method, b-value was calculated using maximum likelihood estimation, and apparent stress was derived from radiated seismic energy and seismic moment. The results indicate that Mc ranges from 3.6 to 5.4 Mw, b-values vary between 0.51 and 2.08, and apparent stress ranges from 0.00 to 0.21 MPa. Low b-values are concentrated around Tijuana Mexicali, whereas the highest apparent stress occurs near La Paz. The limited spatial correspondence between these parameters indicates that earthquake-size distribution and source energetics reflect different aspects of regional. These findings demonstrate that integrating b-value and apparent stress provides complementary information for characterizing regional seismotectonic heterogeneity and improving seismic hazard assessment in active continental rift systems.

Keywords: Gulf of California Rift System; Gutenberg-Richter b-value; apparent stress; seismic hazard; seismotectonic heterogeneity

Acknowledgments

The authors would like to thank the Department of Geophysics, Hasanuddin University, for providing invaluable support, facilities, and opportunities during the course of this research.

Statements and Declarations

Funding

No funding was received for this research.

Competing Interest

The authors have no relevant financial or non-financial interests to disclose.

Author Contributions

All authors contributed equally to the conception, data analysis, and writing of the manuscript.

Data Availability

The earthquake catalogue data used in this study were obtained from the United States Geological Survey (USGS) Earthquake Catalog and are publicly available through the USGS earthquake data portal. Processed datasets supporting the results, including magnitude-completeness, b-value, and apparent-stress estimates, are available from the corresponding author upon reasonable request.

Highlights

- Seismotectonic heterogeneity was assessed using Mc, b-value, and apparent stress.
- Low b-values were concentrated around the Tijuana–Mexicali region.
- The highest apparent stress occurred in the southeastern region near La Paz.
- b-value and apparent stress show limited spatial correspondence.
- Integrated seismic parameters provide complementary insights into rift dynamics.

1. Introduction

Continental rifting is one of the most fundamental geodynamic processes governing the evolution of the Earth's lithosphere because it controls continental breakup, the formation of new ocean basins, and the development of plate boundaries (Brune et al. 2023; Tugend et al. 2024; Yu et al. 2025; Zheng et al. 2026). Unlike subduction zones and mid-ocean ridges, which develop along well-defined plate boundaries, continental rift systems evolve within thick and compositionally heterogeneous continental crust(Barr 2022; Nixon et al. 2026; Sager et al. 2022; Zwaan et al. 2024). Consequently, crustal deformation is controlled by the interaction of tectonic extension, brittle faulting, magmatic intrusion, fluid migration, and variations in crustal rheology (Axen 2024; Jin et al. 2022; Yang et al. 2025). The interaction among these processes produces complex spatial and temporal patterns of crustal deformation, seismic activity, and stress evolution.

One of the most representative examples is the Gulf of California Rift System in northwestern Mexico, which is currently undergoing the transition from continental rifting to oceanic crust formation (Alva-Valdivia et al. 2021; Manatschal et al. 2021). This region accommodates the relative motion between the Pacific Plate and the North American Plate through a tectonic system composed of transform faults, normal faults, and spreading centers (Furlong et al. 2024; Journeau et al. 2026; Tian et al. 2024; Withers et al. 2023; Zhao et al. 2023). The interaction among these tectonic structures generates significant spatial variations in seismicity as a consequence of differences in fault geometry, crustal composition, tectonic loading, magmatic activity, and deformation mechanisms (Abdelfattah et al. 2025; Earth 2026b, 2026a; Zhao et al. 2026). Therefore, evaluating the spatial variability of seismic characteristics associated with stress conditions in the Gulf of California Rift System is essential for improving our understanding of earthquake generation mechanisms and seismic hazard within an actively evolving plate boundary system.

Statistical seismology provides a range of effective approaches for evaluating stress conditions, seismicity patterns, and crustal heterogeneity in tectonically active regions (Abdalzaher et al. 2024; Bi et al. 2026; D'Alessandro 2026). One of the most widely used parameters is the Gutenberg-Richter *b*-value, which describes the relationship between earthquake frequency and magnitude (Boulanouar et al. 2025; Geffers et al. 2023; Islam et al. 2023; Pisarenko et al. 2023; Polat 2022; Raz et al. 2018; Tiwari

& Paudyal 2023; Yamagishi et al. 2021). Spatial variations in *b*-value are commonly interpreted as indicators of differential stress and crustal heterogeneity, where low *b*-values generally reflect higher stress accumulation and an increased likelihood of large-magnitude earthquakes, whereas high *b*-values are typically associated with greater structural heterogeneity and the predominance of small-magnitude events (Chang et al. 2025; Peng et al. 2021; Zafar et al. 2022). However, *b*-value variations are influenced not only by stress conditions but also by geological factors such as temperature, fluid pressure, fracture distribution, and rock properties; therefore, their interpretation should consider the geological setting comprehensively (Gao et al. 2024; Huang et al. 2025; Ma et al. 2026; Mukuhira et al. 2024; Zhu et al. 2021). Another important parameter is apparent stress, which represents the effective stress during earthquake rupture based on the relationship between radiated seismic energy and seismic moment. Unlike the *b*-value, which primarily reflects long-term stress accumulation inferred from earthquake population characteristics, apparent stress characterizes the efficiency of seismic energy release during rupture (Petersen et al. 2022; Wech 2021; Wirth et al. 2022). Consequently, integrating *b*-value and apparent stress provides complementary information by linking stress accumulation prior to earthquake occurrence with energy release during rupture, thereby enabling a more comprehensive assessment of stress evolution within active continental rift systems.

Previous studies have extensively investigated seismicity patterns, crustal deformation, fault behavior, and stress variations in the Gulf of California Rift System as well as in other tectonically active regions (Bonini et al. 2019; Castro et al. 2017, 2018, 2018; Chousianitis et al. 2024; Console et al. 2022; Cruz-Hernández et al. 2023; Johnson et al. 2017; Lizarralde et al. 2007). The *b*-value has been widely applied to identify spatial variations in seismicity and stress conditions, whereas apparent stress has primarily been used to characterize earthquake source properties and seismic energy radiation (Gómez Alba et al. 2020; Nampally et al. 2018; Sainoki et al. 2023). Nevertheless, these two parameters have largely been examined independently, leaving the relationship between stress accumulation and seismic energy release insufficiently understood. Although both parameters provide complementary perspectives, studies integrating *b*-value and apparent stress to characterize the spatial heterogeneity of stress conditions within the Gulf of California Rift System remain relatively limited (Abdelfattah et al. 2020; Danciu et al. 2024; Siino et al. 2018). Such integration is particularly important because regions

experiencing high stress accumulation do not necessarily exhibit similar patterns of seismic energy release. Therefore, the combined application of these two parameters is expected to provide a more comprehensive understanding of earthquake generation processes in continental rift environments.

Based on these considerations, an integrated approach is required to achieve a more comprehensive understanding of stress variations and seismic energy release within active continental rift systems. Therefore, this study integrates Gutenberg-Richter *b*-value and apparent stress analyses to characterize the spatial heterogeneity of seismic parameters that reflect the distribution of tectonic stress within the Gulf of California Rift System. Specifically, this research aims to evaluate the relationship between stress accumulation and seismic energy release, identify zones exhibiting anomalous *b*-value and apparent stress indicative of spatial variations in stress conditions and rupture characteristics, and improve the understanding of seismotectonic evolution during the transition from continental rifting to oceanic crust formation.

2. Method

This study focuses on the Gulf of California Rift System, northwestern Mexico (see Figure 1). The earthquake catalog used in this study was obtained from the United States Geological Survey (USGS) (https://earthquake.usgs.gov/earthquakes/search/), and includes earthquake origin time, epicentral location, focal depth, magnitude, and related seismic parameters for the period 1900-2026. Because this study focuses on shallow crustal seismicity associated with active faulting and rifting, the analysis was restricted to earthquakes with focal depths ≤50 km. This depth range emphasizes seismicity occurring within the brittle crust, where earthquake activity is predominantly associated with active faulting and shallow crustal deformation. Earthquakes occurring at these depths are closely related to brittle faulting and active tectonic processes. Because the USGS catalog contains earthquakes reported using different magnitude scales, all magnitudes were converted to moment magnitude (Mw) to produce a homogeneous earthquake catalog for subsequent statistical analyses. The final dataset contains earthquakes with magnitudes Mw ≤6.

2.1 Declustering Earthquake Data

Prior to the seismotectonic analyses, the earthquake catalog was processed using a declustering procedure to remove dependent events, including aftershocks, foreshocks, and earthquake clusters. The

presence of these dependent events may distort the earthquake frequency magnitude distribution and introduce bias into the estimation of seismic parameters, particularly the Gutenberg-Richter b-value. Declustering was performed using the method proposed by Gardner and Knopoff (1974). This method identifies dependent earthquake sequences based on magnitude-dependent spatial and temporal windows, thereby retaining only statistically independent earthquakes (background seismicity). The resulting declustered catalog was subsequently used for the estimation of the Magnitude of Completeness (Mc), b-value, and apparent stress, ensuring that the analyses represent the regional background seismicity rather than clustered seismic activity.

2.2 Magnitude Completeness Calculation

The Magnitude of Completeness (Mc) was estimated using the Entire Magnitude Range (EMR) method proposed by Woessner and Wiemer (2005). The EMR method models the earthquake frequency-magnitude distribution as a combination of a cumulative normal distribution representing the incomplete portion of the earthquake catalog and an exponential Gutenberg-Richter distribution representing the complete portion. Compared with commonly used approaches such as the Maximum Curvature (MAXC), Mc by Best Stability (MBS), and the Goodness-of-Fit Test (GOF), the EMR method utilizes the entire magnitude range, resulting in a more stable and reliable estimate of Mc, particularly for heterogeneous earthquake catalogs (Wajedy et al. 2026). The estimated Mc was subsequently adopted as the minimum magnitude threshold for all b-value calculations to ensure that only statistically complete earthquake events were included in the analysis.

2.3 b-value Calculation

The relationship between the frequency of earthquake occurrence and earthquake magnitude is represented by the Gutenberg-Richter relationship, which provides the basis for statistical seismicity analysis to characterize the magnitude distribution of earthquakes (Gutenberg & Richter 1956). The relationship is expressed as follows:

$$\log_{10} N(M) = a - bM$$

where $N(M)$ represents the cumulative number of earthquakes with magnitudes greater than or equal to (M), (a) is a constant that describes the level of seismic activity in a region, and (b) is a parameter that controls the relative frequency distribution between small- and large-magnitude earthquakes.

In this study, the spatial distribution of the b-value was estimated using the Maximum Likelihood Estimation (MLE) method proposed by Aki (1965). Before the calculation, only earthquakes with magnitudes greater than or equal to the Magnitude of Completeness M_c were included to ensure that the earthquake catalog was complete for the frequency-magnitude analysis. The b-value was calculated using the following equation (Wajedy et al. 2026):

$$b = \frac{\log e}{\bar{M} - (M_c - \Delta M/2)} \tag{1}$$

where b is the Gutenberg-Richter parameter, M is the mean magnitude of earthquakes with M ≥ M_c, ΔM is the magnitude-bin width, set to 0.1 in this study, and M_c is the magnitude of completeness estimated using the EMR method. The b-value represents the relative proportion of small- and large-magnitude earthquakes within a complete earthquake population. A low b-value indicates a relatively greater proportion of moderate- to large-magnitude earthquakes, whereas a high b-value indicates a relatively greater proportion of small-magnitude earthquakes, including variations in differential stress, fault structure, material heterogeneity, and other geological factors (Wajedy et al. 2026).

2.4 Apparent Stress

Apparent stress is calculated to quantify the efficiency of seismic energy release during earthquake rupture based on the relationship between radiated seismic energy and seismic moment. This parameter represents the proportion of strain energy released as seismic waves during the rupture process and is therefore widely used to evaluate earthquake source characteristics and variations in stress conditions within active tectonic regions. In this study, the spatial distribution of apparent stress was used to identify variations in seismic energy release and was subsequently compared with the b-value distribution to evaluate the relationship between stress accumulation and seismic energy release. Following Wyss (1970), apparent stress was calculated using the following equation:

$$\sigma_a = \mu \frac{E_s}{M_0} \tag{3}$$

where μ is the shear modulus (assumed to be 3×10^{10} Pa), E_s is the radiated seismic energy, and M_0 represents seismic moment. These two parameters describe the relationship between the seismic energy

released during the rupture process and the size of the earthquake source in the calculation of apparent stress.

The radiated seismic energy E_s was estimated using the empirical relationship developed by Gutenberg and Richter (1956), which relates Moment Magnitude Mw to radiated seismic energy. The relationship is expressed as follows (Wajedy et al., 2026):

$$\log E_s = 1.5\left(\frac{M_w - 2.476}{0.6016}\right) + 11.8 \tag{4}$$

where E_s represents the radiated seismic energy expressed in joules. This equation was used to estimate the amount of seismic energy released during the rupture process, allowing the resulting energy values to be used as the basis for calculating apparent stress.

The seismic moment M_0 was calculated using the empirical relationship between Moment Magnitude M_s and seismic moment as follows:

$$M_0 = 10^{(1.5M_w + 16.1)} \tag{5}$$

where M_0 is the seismic moment expressed in dyne·cm. This parameter represents the size of the earthquake source and was used together with the radiated seismic energy to obtain apparent stress values, allowing the efficiency of seismic energy release for individual earthquake events to be quantitatively evaluated. To obtain a spatial distribution that could be directly compared with the b-value, the apparent stress calculation was performed using the same moving-window configuration, with a search radius of 50 km and a minimum of 20 earthquake events at each calculation point (Wajedy et al. 2026; Wajedy 2026). Using an identical configuration ensures that both parameters are calculated from comparable earthquake populations, allowing their spatial relationship to be evaluated consistently.

3. Results

3.1 Magnitude Completeness Distribution

The spatial distribution of the magnitude of completeness (M_c) obtained using the Entire Magnitude Range (EMR) method shows clear heterogeneity across the Gulf of California Rift System (see Figure 2). The M_c values range from 3.6 to 5.4 Mw, with a regional difference of approximately 1.8 magnitude units. The lowest Mc values, approximately 3.6-4.1 Mw, are concentrated in the northern part of the

study area, particularly around Tijuana, Mexicali, and San Felipe, whereas higher values, approximately 4.8-5.4 Mw, are mainly observed in the southern part, particularly around La Paz and the southeastern Gulf of California.

This pattern indicates that earthquake catalog completeness is not spatially uniform. The northern region has a lower completeness threshold, allowing smaller-magnitude earthquakes to be included in the population of earthquakes considered complete. In contrast, the higher Mc values in the southern part indicate that a higher magnitude threshold is required in this region to obtain an earthquake population that can be considered complete. This spatial pattern of Mc provides the basis for determining the magnitude threshold in the subsequent analysis, particularly the b-value analysis, to minimize the influence of catalog incompleteness on the analytical results.

3.2 b-Value Analysis

The spatial distribution of the Gutenberg-Richter b-value shows strong heterogeneity throughout the study area, with values ranging from 0.51 to 2.08 (see Figure 3). The zones with the lowest values, approximately 0.51-0.80, are mainly concentrated in the northern part, particularly around Tijuana, Mexicali, and San Felipe. In contrast, higher b-values, approximately 1.50-2.08, are mainly distributed in the central to southern parts of the study area, including the areas around Guerrero Negro, Santa Rosalía, and parts of La Paz.

The range of approximately 1.57 b-value units indicates significant differences in the characteristics of the earthquake magnitude-frequency relationship across the study area. The low b-value zones in the northern part indicate an earthquake population with a relatively greater proportion of moderate- to large-magnitude events within the magnitude range that has been considered complete. Conversely, zones with higher b-values show a relatively greater proportion of small-magnitude events. These variations indicate differences in seismicity characteristics between zones, which subsequently need to be interpreted by considering the Mc distribution and the seismotectonic conditions of the study area.

3.3 Apparent Stress Estimation

The spatial distribution of apparent stress shows a different pattern compared with the b-value distribution (see Figure 4). Apparent stress values range from approximately 0.00 to 0.21 MPa. Low values, generally <0.05 MPa, are concentrated in the northern part, particularly around Tijuana and

Mexicali, whereas the highest values, approximately 0.18-0.21 MPa, occur in the southeastern part, particularly around La Paz and the southern Gulf of California. The difference between the low apparent stress domain in the north and the high domain in the southeast reaches approximately 0.16 MPa.

The apparent stress distribution indicates that the characteristics of seismic energy release are not uniform throughout the study area. Zones with relatively high apparent stress show greater seismic energy release characteristics compared with zones with low apparent stress. This pattern is subsequently compared with the b-value distribution to determine whether zones showing low b-values also exhibit high apparent stress. This comparison is necessary because b-value and apparent stress represent different characteristics of seismicity.

4. Discussion

The Gulf of California is an active tectonic region characterized by complex fault systems and crustal deformation (Goff et al. 1987; Higa et al. 2022; Martín-Barajas et al. 2013). These tectonic conditions produce spatial variations in seismic activity and earthquake source characteristics (Fletcher & Munguia 2000; Hauksson et al. 2014). The Gulf of California's tectonic complexity, with plate motion partitioned across spreading centers, transform faults, and margin-normal faults (Fletcher & Munguía 2000), produces distinct seismic behaviors in different fault domains. This explains why b-value and apparent stress distributions do not always coincide, as earthquake-size statistics and rupture energetics are controlled by separate tectonic regimes. Therefore, analyses of Magnitude of Completeness (Mc), b-value, and apparent stress are important for evaluating variations in seismicity characteristics across the study area (Tourani et al. 2024)

The results of the Magnitude of Completeness (M_c) analysis using the Entire Magnitude Range (EMR) method show spatial variations in Mc across the study area (see Figure 2). The M_c-EMR distribution shows M_c values ranging from 3.6 to 5.4 Mw, with a difference of approximately 1.8 magnitude units between the lowest and highest values. Relatively low M_c values are concentrated in the northern part of the study area, particularly around Tijuana and Mexicali, with values of approximately 3.6-4.0 Mw, whereas around San Felipe, M_c increases to approximately 4.0-4.2 Mw. In contrast, M_c values become progressively higher toward the south and southeast, with values of approximately 4.8-5.2 Mw across

most of Baja California Sur and reaching approximately 5.2-5.4 Mw in the southeastern part of the study area. Thus, there is a difference of approximately 1.8 Mw between the lowest and highest Mc values. Lower M_c values (3.6-4.0 M_w) indicate that relatively small-magnitude earthquakes can be detected and more completely represented in the catalog, whereas higher Mc values (5.0-5.4 M_w indicate that smaller-magnitude events are relatively more difficult to detect completely in these areas (Ahadov & Ozturk 2022; Chasanah & Handoyo 2021). This spatial variation in Mc indicates differences in the level of catalog completeness between regions, which need to be considered when interpreting the distributions of b-value and apparent stress.

The frequency magnitude distribution of earthquakes follows the Gutenberg Richter law, in which the b-value represents the slope of the relationship between earthquake frequency and magnitude (Godano et al. 2014). The b-value distribution shows relatively clear spatial variations (see Figure 3). Zones with b-values <1 are mainly found around Tijuana and Mexicali, whereas b-values >1 occur in several other parts of the study area, as shown in the b-value figure. The b-values within the study area range from 0.51 to 2.08, resulting in a difference of approximately 1.57 between the lowest and highest values. Low b-value zones, particularly within the range of 0.51-0.80, indicate a relatively greater dominance of moderate- to large-magnitude events compared with areas characterized by high b-values (Schorlemmer et al. 2005). Low b-values are commonly associated with relatively high differential stress conditions (Gulia & Wiemer 2010; Scholz 2015). In Tijuana and Mexicali, the low b-value zone develops in the northern Gulf of California, which is influenced by active fault systems, including the Cerro Prieto Fault and Imperial Fault (Castro et al. 2017; Fletcher & Munguia 2000). The presence of low b-values within this fault domain indicates that variations in earthquake magnitude distribution may be related to local deformation characteristics and fault structures. Conversely, b-values >1 indicate a relatively greater dominance of small-magnitude earthquakes in the catalog (Enescu & Ito 2002; Gulia et al. 2018; Schorlemmer et al. 2005). These differences demonstrate that seismicity characteristics are not uniform throughout the study area.

The apparent stress distribution shows a pattern that does not completely coincide with the b-value distribution (see Figure 4). Relatively low apparent stress, generally < 0.05 MPa, is found around Tijuana and Mexicali, although this region is characterized by low b-values in the range of 0.51-0.80.

In contrast, relatively high apparent stress develops in the southeastern part of the study area, particularly around La Paz, with values reaching approximately 0.18-0.21 MPa. The difference between the low values in the northern part and the highest values in the southeast reaches approximately 0.16 MPa. This pattern differs from the b-value distribution because the lowest b-values are found in the northern part, whereas the highest apparent stress occurs in the southeastern part. Theoretically, low b-values are often associated with relatively high stress conditions, and therefore these zones might be expected to exhibit higher apparent stress (Wajedy et al. 2026). However, this condition is not observed in the present results.

This difference becomes clearer when the apparent stress distribution is compared with the M_c-EMR distribution. Around Tijuana and Mexicali, the b-value ranges from 0.51 to 0.80, apparent stress is generally < 0.05 MPa, and M_c is relatively low at approximately 3.6-4.1 M_w. These three parameters occur in relatively similar locations. This combination indicates that the low b-value zone around Tijuana and Mexicali is not automatically accompanied by high apparent stress (Ahadov & Ozturk 2022). The relatively low M_c also indicates that the catalog in this region is capable of capturing smaller-magnitude events. Therefore, the low b-values around Tijuana and Mexicali need to be interpreted by considering the level of catalog completeness and local seismicity patterns, rather than solely as an indicator of high-stress conditions.

A different pattern is observed in the southeastern part of the study area. Around La Paz, apparent stress reaches 0.18-0.21 MPa, whereas the zone with the lowest b-values does not occur in the same location. The spatial difference between the two parameters indicates that earthquake magnitude distributions and apparent stress do not always follow the same pattern (Baltay et al. 2011; Oth 2013). Thus, zones with a relatively greater proportion of moderate- to large-magnitude events based on b-value are not necessarily the zones with the highest apparent stress. This result emphasizes the heterogeneity of seismicity characteristics across different parts of the study area (Wajedy 2026; Wajedy & Massinai 2026).

These results can be compared with previous studies showing that low b-values are associated with relatively high stress conditions and a greater dominance of larger-magnitude earthquakes in active tectonic regions (Schorlemmer et al. 2005). The similarity with these studies is reflected in the presence

of b-values of 0.51-0.80 around Tijuana and Mexicali. This result supports the use of b-value as one parameter for evaluating variations in earthquake magnitude distribution characteristics.

However, when compared with apparent stress, the pattern obtained in this study shows an inconsistent spatial relationship. The low b-value zone around Tijuana and Mexicali does not coincide with the high apparent stress zone. Conversely, the highest apparent stress values, approximately 0.18-0.21 MPa, develop in the southeastern part of the study area. This difference may be related to local tectonic conditions, earthquake distribution, earthquake source characteristics, catalog period, and the methods used to estimate each parameter (Allmann & Shearer 2009; Baltay et al. 2011; Oth 2013; Rigorous et al. 1986).

This condition indicates that b-value should not be used as the sole parameter for identifying areas with high-stress conditions or earthquake hazard potential. (Chang et al. 2025; El-Isa & Eaton 2014). Although a zone with b-values of 0.51-0.80 is found around Tijuana and Mexicali, this region does not show high apparent stress. Conversely, the highest apparent stress is found in the southeastern part. These results show that b-value and apparent stress provide different information regarding earthquake characteristics and earthquake sources. Therefore, the interpretation of seismotectonic conditions becomes stronger when both parameters are evaluated together while considering Mc and the characteristics of the tectonic structures (Bonini et al. 2019; Mousavi et al. 2026).

Therefore, areas with low b-values remain important for seismic monitoring, but earthquake hazard assessment cannot be based solely on b-values. Mc, apparent stress, fault activity, focal mechanisms, and other tectonic parameters need to be considered together. studies may integrate these parameters with crustal deformation data to examine the relationship between fault activity, earthquake distribution, and earthquake source characteristics in greater detail.

The variations in b-value, apparent stress, and Mc obtained in this study are also related to the complexity of the geological structures and tectonic system of the Gulf of California. The low b-value zone around Tijuana and Mexicali occurs in an area influenced by the Cerro Prieto and Imperial fault systems and associated fault structures, whereas high apparent stress develops in the southeastern part, particularly around La Paz. These differences indicate that seismicity characteristics may vary between tectonic domains. Integration of seismological results with geological and fault-structure information is

therefore needed to determine whether the contrast between the northern and southeastern parts is primarily related to differences in earthquake source characteristics, fault structures, or the level of catalog completeness.

5. Conclusions

This study success to characterize the spatial heterogeneity of stress conditions in the Gulf of California Rift System through the integration of Magnitude of Completeness (Mc), Gutenberg-Richter b-value, and apparent stress analyses. The results show that Mc values vary between 3.6-5.4 Mw, with lower values in the northern part and increasing toward the south, indicating differences in earthquake catalog completeness between regions. The b-value distribution ranges from 0.51-2.08, with low b-value zones concentrated around Tijuana and Mexicali, whereas higher values develop in the central to southern parts. In contrast, apparent stress ranges from 0.00-0.21 MPa, with the maximum values found around La Paz, resulting in a spatial pattern that does not coincide with the b-value distribution. These results indicate that zones with low b-values are not always associated with high apparent stress, suggesting that the relationship between stress accumulation and seismic energy release in a continental rift system is neither simple nor linear. This finding provides a scientific contribution in the form of evidence that the integration of Mc, b-value, and apparent stress can reveal seismotectonic heterogeneity that cannot be adequately explained using a single seismic parameter. Therefore, this multiparameter approach provides a more comprehensive basis for interpreting variations in stress, earthquake source characteristics, and deformation evolution in an active continental rift environment. The implication of this study is that earthquake hazard assessment in the Gulf of California Rift System and other active tectonic regions should not rely solely on b-value distributions, but should also consider apparent stress, earthquake catalog completeness, and geological and fault-structure information to obtain a more reliable interpretation of seismotectonic conditions.

References

Abdalzaher MS, Moustafa SSR, Yassien M (2024) Development of smoothed seismicity models for seismic hazard assessment in the Red Sea region. Nat Hazards 120:12515–12544. https://doi.org/10.1007/s11069-024-06695-x

Abdelfattah A, Jallouli C, Alzahrani H, Qaysi S, Fnais M, Al-Amri A (2025) Exploring the potential location of future earthquakes in Harrat Lunayyir, Western Saudi Arabia. All Earth 37:1–18. https://doi.org/10.1080/27669645.2025.2454711

Abdelfattah AK, Jallouli C, Qaysi S, Al-Qadasi B (2020) Crustal stress in the Northern Red Sea region as inferred from seismic b-values, seismic moment release, focal mechanisms, gravity, magnetic, and heat flow data. Surv Geophys 41:963–986. https://doi.org/10.1007/s10712-020-09602-8

Ahadov B, Ozturk S (2022) Spatial variations of fundamental seismotectonic parameters for the earthquake occurrences in the Eastern Mediterranean and Caucasus. Nat Hazards 111:2177–2192. https://doi.org/10.1007/s11069-021-05170-1

Allmann BP, Shearer PM (2009) Global variations of stress drop for moderate to large earthquakes. J Geophys Res Solid Earth 114:1–22. https://doi.org/10.1029/2008JB005821

Alva-Valdivia LM, Vidal-Solano JR, Velderrain-Rojas LA, González-Rangel JA (2021) Rock magnetic characterization and paleomagnetic directional analysis of Isla San Pedro Nolasco dikes, Gulf of California, Mexico. Bull Volcanol 83. https://doi.org/10.1007/s00445-021-01477-w

Axen G (2024) Geochemical, mineralogical, and fluid processes in the brittle-plastic transition of continental crust. Geochem Geophys Geosyst 25. https://doi.org/10.1029/2024GC011446

Baltay A, Ide S, Prieto G, Beroza G (2011) Variability in earthquake stress drop and apparent stress. Geophys Res Lett 38:1–6. https://doi.org/10.1029/2011GL046698

Barr S (2022) GAC-MAC-IAH-CNC-CSPG 2022 Halifax Meeting: Abstracts, Volume 45. Geosci Can 49:59–226. https://doi.org/10.12789/geocanj.2022.49.188

Bi J, Li Y, Pan Y (2026) Spatiotemporal characteristics and geophysical drivers of the fractal dimension and b-value in North China seismicity. PLoS One 21:1–16. https://doi.org/10.1371/journal.pone.0349558

Bonini M, Cerca M, Moratti G, López-Martínez M, Corti G, Gracia-Marroquín D (2019) Strain

partitioning in highly oblique rift settings: Inferences from the southwestern margin of the Gulf of California (Baja California Sur, México). Tectonics 38:4426–4453. https://doi.org/10.1029/2019TC005566

Boulanouar A, Khalil A, Sebbani J, Ouali AE, Rahmouni A (2025) Geographic distribution of the b-value in north Morocco and its surrounding for seismic zones identification. Jordan J Earth Environ Sci 16:11–16.

Brune S, Potsdam GFZ, Ldeo FK (2023) NREE_RiftReview_Version3_fin-1. 1–19.

Castro RR, Mendoza-Camberos A, Pérez-Vertti A (2018) Radiated seismic energy of earthquakes in the south-central region of the Gulf of California, Mexico. Geophys J Int 214:990–1003. https://doi.org/10.1093/GJI/GGY178

Castro RR, Stock JM, Hauksson E, Clayton RW (2017) Active tectonics in the Gulf of California and seismicity (M > 3.0) for the period 2002–2014. Tectonophysics 719–720:4–16. https://doi.org/10.1016/j.tecto.2017.02.015

Chang Y, Wang R, Han P, Wang J, Miao M, Zeng Z, Wu W, Jiang C, Meng L, Shi H, Hattori K (2025) b-value evaluation and applications to seismic hazard assessment. Entropy 27:1–19. https://doi.org/10.3390/e27090958

Chasanah U, Handoyo E (2021) Determination the magnitude of completeness, b-value and a-value for seismicity analysis in East Java, Indonesia. J Phys Conf Ser 1805. https://doi.org/10.1088/1742-6596/1805/1/012009

Chousianitis K, Sboras S, Mouslopoulou V, Chouliaras G, Hristopulos DT (2024) The upper crustal deformation field of Greece inferred from GPS data and its correlation with earthquake occurrence. J Geophys Res Solid Earth 129. https://doi.org/10.1029/2023JB028004

Console R, Carluccio R, Murru M, Papadimitriou E, Karakostas V (2022) Physics-based simulation of spatiotemporal patterns of earthquakes in the Corinth Gulf, Greece, fault system. Bull Seismol Soc Am 112:98–117. https://doi.org/10.1785/0120210038

Cruz-Hernández F, Castro-Escamilla RR, Mendoza-Camberos JA, Pérez-Vertti A (2023) Seismicity and state of stress in the north-central region of the Gulf of California, Mexico. Tectonophysics 863. https://doi.org/10.1016/j.tecto.2023.230020

D'Alessandro A (2026) Tectonic, depth, and magnitude controls on global earthquake stress drop. Solid Earth Sci 11:100324. https://doi.org/10.1016/j.sesci.2026.100324

Danciu L, Giardini D, Weatherill G, Basili R, Nandan S, Rovida A, Beauval C, Bard PY, Pagani M, Reyes CG, Sesetyan K, Vilanova S, Cotton F, Wiemer S (2024) The 2020 European Seismic Hazard Model: overview and results. Nat Hazards Earth Syst Sci 24:3049–3073. https://doi.org/10.5194/nhess-24-3049-2024

Earth C (2026a) Communications Earth & Environment article in press: Fault-controlled magma pathways driving seismicity and eruption risk in Eastern Turkey. Tomography reveals two shallow magma reservoirs beneath the Erzincan.

Earth C (2026b) Communications Earth & Environment article in press: Seismic effects of deep crustal high-density material in the southeastern Korean Peninsula.

El-Isa ZH, Eaton DW (2014) Spatiotemporal variations in the b-value of earthquake magnitude-frequency distributions: Classification and causes. Tectonophysics 615–616:1–11. https://doi.org/10.1016/j.tecto.2013.12.001

Enescu B, Ito K (2002) Spatial analysis of the frequency-magnitude distribution and decay rate of aftershock activity of the 2000 Western Tottori Earthquake. Earth Planets Space 54:847–859. https://doi.org/10.1186/BF03352077

Fletcher JM, Munguia L (2000) Seafloor spreading in the Gulf of California of Baja California. Geologic evolution of the Gulf of Alarc6n. Tectonics 19:1107–1123.

Furlong KP, Villaseñor A, Benz HM, McKenzie KA (2024) Formation and evolution of the Pacific-North American (San Andreas) plate boundary: Constraints from the crustal architecture of Northern California. Tectonics 43. https://doi.org/10.1029/2023TC007963

Gao Q, Ma L, Liu W, Khan NM, Alarifi SS, Sazid M, Inqiad WB (2024) Method for rock fracture prediction and early warning: Insight from fusion of multi-physics field information. Heliyon 10. https://doi.org/10.1016/j.heliyon.2024.e30660

Geffers GM, Main IG, Naylor M (2023) Accuracy and precision of frequency-size distribution scaling parameters as a function of dynamic range of observations: Example of the Gutenberg-Richter law b-value for earthquakes. Geophys J Int 232:2080–2086. https://doi.org/10.1093/gji/ggac436

Godano C, Lippiello E, De Arcangelis L (2014) Variability of the b value in the Gutenberg-Richter distribution. Geophys J Int 199:1765–1771. https://doi.org/10.1093/gji/ggu359

Goff JA, Bergman EA, Solomon SC (1987) Earthquake source mechanisms and transform fault tectonics in the Gulf of California. J Geophys Res 92. https://doi.org/10.1029/jb092ib10p10485

Gómez Alba S, Vargas CA, Zang A (2020) Evidencing the relationship between injected volume of water and maximum expected magnitude during the Puerto Gaitán (Colombia) earthquake sequence from 2013 to 2015. Geophys J Int 220:335–344. https://doi.org/10.1093/gji/ggz433

Gulia L, Rinaldi AP, Tormann T, Vannucci G, Enescu B, Wiemer S (2018) The effect of a mainshock on the size distribution of the aftershocks. Geophys Res Lett 45:13277–13287. https://doi.org/10.1029/2018GL080619

Gulia L, Wiemer S (2010) The influence of tectonic regimes on the earthquake size distribution: A case study for Italy. Geophys Res Lett 37:1–6. https://doi.org/10.1029/2010GL043066

Hauksson E, Kanamori H, Stock J, Cormier MH, Legg M (2014) Active Pacific North America plate boundary tectonics as evidenced by seismicity in the oceanic lithosphere offshore Baja California, Mexico. Geophys J Int 196:1619–1630. https://doi.org/10.1093/gji/ggt467

Higa JT, Brown ND, Moon S, Stock JM, Sabbeth L, Bennett SEK, Martín-Barajas A, Argueta MO (2022) Microcontinent breakup and links to possible plate boundary reorganization in the Northern Gulf of California, México. Tectonics 41:1–18. https://doi.org/10.1029/2021TC006933

Huang H, Zhou Y, Zhang Y, Wang C, Bi J (2025) Anisotropic crack evolution and fractal failure mechanism of Lushan shale under compression: Insights from acoustic emission. Sci Rep 15:1–25. https://doi.org/10.1038/s41598-025-98695-5

Islam ARMT, Akter MY, Amanat S, Alam E, Sultana ML, Shahid S, Das A, Peu SD, Mallick J (2023) Assessing seismicity in Bangladesh: An application of Guttenberg-Richter relationship and spectral analysis. Geomat Nat Hazards Risk 14. https://doi.org/10.1080/19475705.2023.2247138

Jin S, Sheng Y, Comeau MJ, Becken M, Wei W, Ye G, Dong H, Zhang L (2022) Relationship of the crustal structure, rheology, and tectonic dynamics beneath the Lhasa-Gangdese Terrane (Southern Tibet) based on a 3-D electrical model. J Geophys Res Solid Earth 127:1–24. https://doi.org/10.1029/2022JB024318

Johnson CW, Fu Y, Bürgmann R (2017) Stress models of the annual hydrospheric, atmospheric, thermal, and tidal loading cycles on California faults: Perturbation of background stress and changes in seismicity. J Geophys Res Solid Earth 122:10605–10625. https://doi.org/10.1002/2017JB014778

Journeau C, Thomas AM, Abercrombie RE, Hirao BW, Liu M, Kuna V (2026) OBS data mining reveals seismic structure and dynamics of the oceanic Blanco Transform Fault, Northeast Pacific. J Geophys Res Solid Earth 131:1–24. https://doi.org/10.1029/2025JB032982

Lizarralde D, Axen GJ, Brown HE, Fletcher JM, González-Fernández A, Harding AJ, Holbrook WS, Kent GM, Paramo P, Sutherland F, Umhoefer PJ (2007) Variation in styles of rifting in the Gulf of California. Nature 448:466–469. https://doi.org/10.1038/nature06035

Ma K, Jiao Z, Wang K, Karakus M (2026) Analysis of microseismic evolution law and damage zone detection in oil storage caverns during operational period. Tunn Undergr Space Technol 172. https://doi.org/10.1016/j.tust.2026.107574

Manatschal G, Chenin P, Lescoutre R, Miró J, Cadenas P, Saspiturry N, Masini E, Chevrot S, Ford M, Jolivet L, Mouthereau F, Thinon I, Issautier B, Calassou S (2021) The role of inheritance in forming rifts and rifted margins and building collisional orogens: A Biscay-Pyrenean perspective. BSGF Earth Sci Bull 192. https://doi.org/10.1051/bsgf/2021042

Martín-Barajas A, González-Escobar M, Fletcher JM, Pacheco M, Oskin M, Dorsey R (2013) Thick deltaic sedimentation and detachment faulting delay the onset of continental rupture in the Northern Gulf of California: Analysis of seismic reflection profiles. Tectonics 32:1294–1311. https://doi.org/10.1002/tect.20063

Mousavi MH, Jalooli P, Talebi A (2026) A comprehensive analysis of spatio-temporal seismicity parameters in the Kope-Dagh Region. J Seismol 30. https://doi.org/10.1007/s10950-026-10414-3

Mukuhira Y, Fehler MC, Bjarkason EK, Ito T, Asanuma H (2024) On the b-value dependency of injection-induced seismicity on geomechanical parameters. Int J Rock Mech Min Sci 174.

Nampally S, Padhy S, Dimri VP (2018) Characterizing spatial heterogeneity based on the b-value and fractal analyses of the 2015 Nepal earthquake sequence. Tectonophysics 722:154–162. https://doi.org/10.1016/j.tecto.2017.11.004

Nixon CA, Birch S, Chatain A, Cockell C, Farnsworth KK, Higgins PM, Le Mouélic S, Lopes RMC,

Malaska MJ, Melwani Daswani M, Miller KE, Neish CD, Podlaha OG, Radebaugh J, Schurmeier LR, Schoenfeld A, Soderlund KM, Solomonidou A, Sotin C, et al (2026) Terrestrial analogs to Titan for geophysical research. Rev Geophys 64:1–76. https://doi.org/10.1029/2025RG000909

Oth A (2013) On the characteristics of earthquake stress release variations in Japan. Earth Planet Sci Lett 377–378:132–141. https://doi.org/10.1016/j.epsl.2013.06.037

Peng W, Marsan D, Chen KH, Pathier E (2021) Earthquake swarms in Taiwan: A composite declustering method for detection and their spatial characteristics. Earth Planet Sci Lett 574:117160. https://doi.org/10.1016/j.epsl.2021.117160

Petersen MD, Shumway AM, Powers PM, Moschetti MP, Llenos AL, Michael AJ, Mueller CS, Frankel AD, Rezaeian S, Rukstales KS, McNamara DE, Okubo PG, Zeng Y, Jaiswal KS, Ahdi SK, Altekruse JM, Shiro BR (2022) 2021 US National Seismic Hazard Model for the State of Hawaii. Earthq Spectra 38:865–916. https://doi.org/10.1177/87552930211052061

Pisarenko VF, Skorkina AA, Rukavishnikova TA (2023) Choosing the magnitude range for estimating the b-value. J Volcanol Seismol 17:75–82. https://doi.org/10.1134/S0742046323700124

Polat G (2022) Spatial analysis of b-value variability in Elazig city and the surrounding area (Eastern Turkey). Acta Geophys 70:15–25. https://doi.org/10.1007/s11600-021-00694-3

Raz R, Levine H, Pinto O, Broday DM, Weisskopf Y, Weisskopf MG (2018) It Sc It Sc. Am J Epidemiol 187:717–725.

Rigorous A, For M, Brown THE (1986) N.(t) = fo " f t) da. J ~, Oa. Population (English Edition) 28:103–116.

Sager W, Hoernle K, Höfig TW (2022) Expedition 391 preliminary report: Walvis Ridge Hotspot. 391.

Sainoki A, Schwartzkopff AK, Jiang L, Mitri H (2023) Numerical modelling of spatially and temporally distributed on-fault induced seismicity: Implication for seismic hazards. Int J Coal Sci Technol 10:1–16. https://doi.org/10.1007/s40789-022-00560-7

Scholz CH (2015) On the stress dependence of the earthquake b value. Geophys Res Lett 42:1399–1402. https://doi.org/10.1002/2014GL062863

Schorlemmer D, Wiemer S, Wyss M (2005) Variations in earthquake-size distribution across different stress regimes. Nature 437:539–542. https://doi.org/10.1038/nature04094

Siino M, Alessandro AD, Adelfio G, Scudero S, Chiodi M (2018) SEQUENCES. https://doi.org/10.441/ag-7711

Tian X, Behn MD, Ito G, Schierjott JC, Kaus BJP, Popov AA (2024) Magmatism controls global oceanic transform fault topography. Nat Commun 15:1–9. https://doi.org/10.1038/s41467-024-46197-9

Tiwari RK, Paudyal H (2023) Spatial mapping of b-value and fractal dimension prior to November 8, 2022 Doti Earthquake, Nepal. PLoS One 18:1–13. https://doi.org/10.1371/journal.pone.0289673

Tourani M, Isik V, Saber R, Caglayan A, Chitea F (2024) Evaluation of seismicity and seismotectonics in the Alborz Mountains: Insights from seismic parameters, Northern Iran. J Seismol 28. https://doi.org/10.1007/s10950-024-10218-3

Tugend J, Mohn G, Duretz T, Petri B, Pourhiet LL (2024) Extension of continental lithosphere in rifted margins: A review of thinning mechanisms. C R Geosci 356. https://doi.org/10.5802/crgeos.257

Wajedy MF (2026) Probabilistic insights into seismic activation and quiescence across the East African rift system: Bayesian constraints on continental extension dynamics. Phys Chem Earth 144:104511. https://doi.org/10.1016/j.pce.2026.104511

Wajedy MF, Saaduddin, Massinai MA, Fahruddin F, Thariq A (2026) Seismic hazard and tectonic stress in Halmahera, Indonesia based on b-value and apparent stress analyses. Phys Earth Planet Inter 372:107512. https://doi.org/10.1016/j.pepi.2026.107512

Wajedy MF, Massinai MA (2026) Seismotectonic characterization of Central Sulawesi, Indonesia, using Bayesian b-value estimation and k-means clustering. J Asian Earth Sci 107245.

Wech AG (2021) Cataloging tectonic tremor energy radiation in the Cascadia Subduction Zone. J Geophys Res Solid Earth 126:1–20. https://doi.org/10.1029/2021JB022523

Wirth EA, Sahakian VJ, Wallace LM, Melnick D (2022) The occurrence and hazards of great subduction zone earthquakes. Nat Rev Earth Environ 3:125–140. https://doi.org/10.1038/s43017-021-00245-w

Withers M, Cruden AR, Quigley MC (2023) The development of fault networks at the termination of continental transform faults when their connecting plate boundary is “misaligned.” Tectonics 42:1–19. https://doi.org/10.1029/2023TC007823

Yamagishi Y, Saito K, Hirahara K, Ueda N (2021) Spatio-temporal clustering of earthquakes based on

distribution of magnitudes. Appl Netw Sci 6. https://doi.org/10.1007/s41109-021-00413-3

Yang P, Pérez-Gussinyé M, Liu S, García-Pintado J, RaghuRam G (2025) Interactions between syn-rift magmatism and tectonic extension at intermediate rifted margins. Earth Planet Sci Lett 671. https://doi.org/10.1016/j.epsl.2025.119682

Yu AJ, Gün E, McCaffrey KJW, Heron PJ (2025) A recipe for exotic continental fragment formation: Key constraints from numerical rift models. J Geophys Res Solid Earth 130. https://doi.org/10.1029/2024JB030041

Zafar S, Hedayat A, Moradian O (2022) Micromechanics of fracture propagation during multistage stress relaxation and creep in brittle rocks. Rock Mech Rock Eng 55:7611–7627. https://doi.org/10.1007/s00603-022-03045-w

Zhao L, Zhan Y, Hu Y, Tang J, Cao C, Wang Q, Sun X (2026) Three-dimensional electrical structure beneath the Changbaishan volcano (NE China): Implications for magmatic plumbing systems and diverse eruption styles. Geosci Front 17:102340. https://doi.org/10.1016/j.gsf.2026.102340

Zhao S, McClusky S, Cummins PR, Miller MS, Nugroho H (2023) New insights into crustal deformation of the Indonesia–Australia–New Guinea collision zone from a broad-scale kinematic model. J Geophys Res Solid Earth 128. https://doi.org/10.1029/2022JB024810

Zheng Y, Chen R, Chen Y, Dai L, Gao X, Xia Q (2026) From plate margins to continental interiors: Theoretical reconstruction and paradigm breakthrough. Sci China Earth Sci 69:2435–2456. https://doi.org/10.1007/s11430-026-1975-9

Zhu Q, Zhao X, Westman E (2021) Review of the evolution of mining-induced stress and the failure characteristics of surrounding rock based on microseismic tomography. Shock Vib 2021. https://doi.org/10.1155/2021/2154857

Zwaan F, Alves TM, Cadenas P, Gouiza M, Phethean JJJ, Brune S, Glerum AC (2024) (D)rifting in the 21st century: Key processes, natural hazards, and geo-resources. Solid Earth 15:989–1028. https://doi.org/10.5194/se-15-989-2024

Figure Caption

Fig. 1. Spatial distribution of earthquake epicenters and major fault systems across the Gulf of California Rift System, northwestern Mexico, during the period 1900-2026, highlighting the spatial association between seismicity and active fault structures associated with regional rifting and tectonic deformation.

Fig. 2. Spatial distribution of the magnitude of completeness (M_c) estimated using the Empirical Magnitude Range (EMR) method with a 50-km moving window and a minimum of 20 earthquakes per analysis location across the Gulf of California Rift System, Mexico.

Fig. 3. Spatial distribution of the b-value estimated from earthquakes above the locally determined magnitude of completeness (M_c) using a 50-km moving window across the Gulf of California Rift System, Mexico.

Fig. 4. Spatial distribution of apparent stress estimated from the locally complete earthquake populations using a 50-km moving window across the Gulf of California Rift System, Mexico.

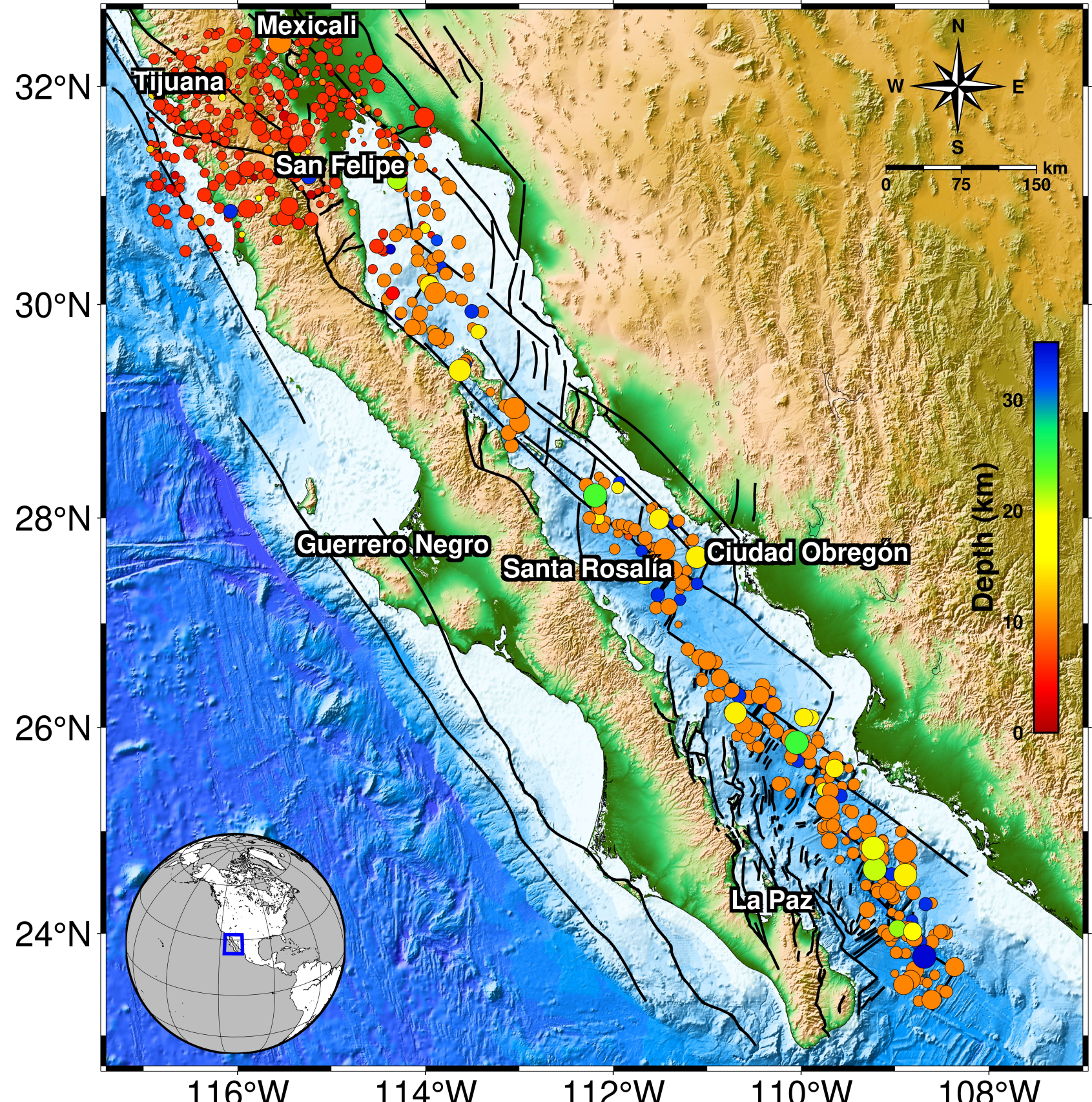
Mexicali
Tijuana
San Felipe
Guerrero Negro
Santa Rosalía
Ciudad Obregón
La Paz
N
W
E
S
km
0
75
150
Depth (km)
30
20
10
0
32°N
30°N
28°N
26°N
24°N
116°W
114°W
112°W
110°W
108°W

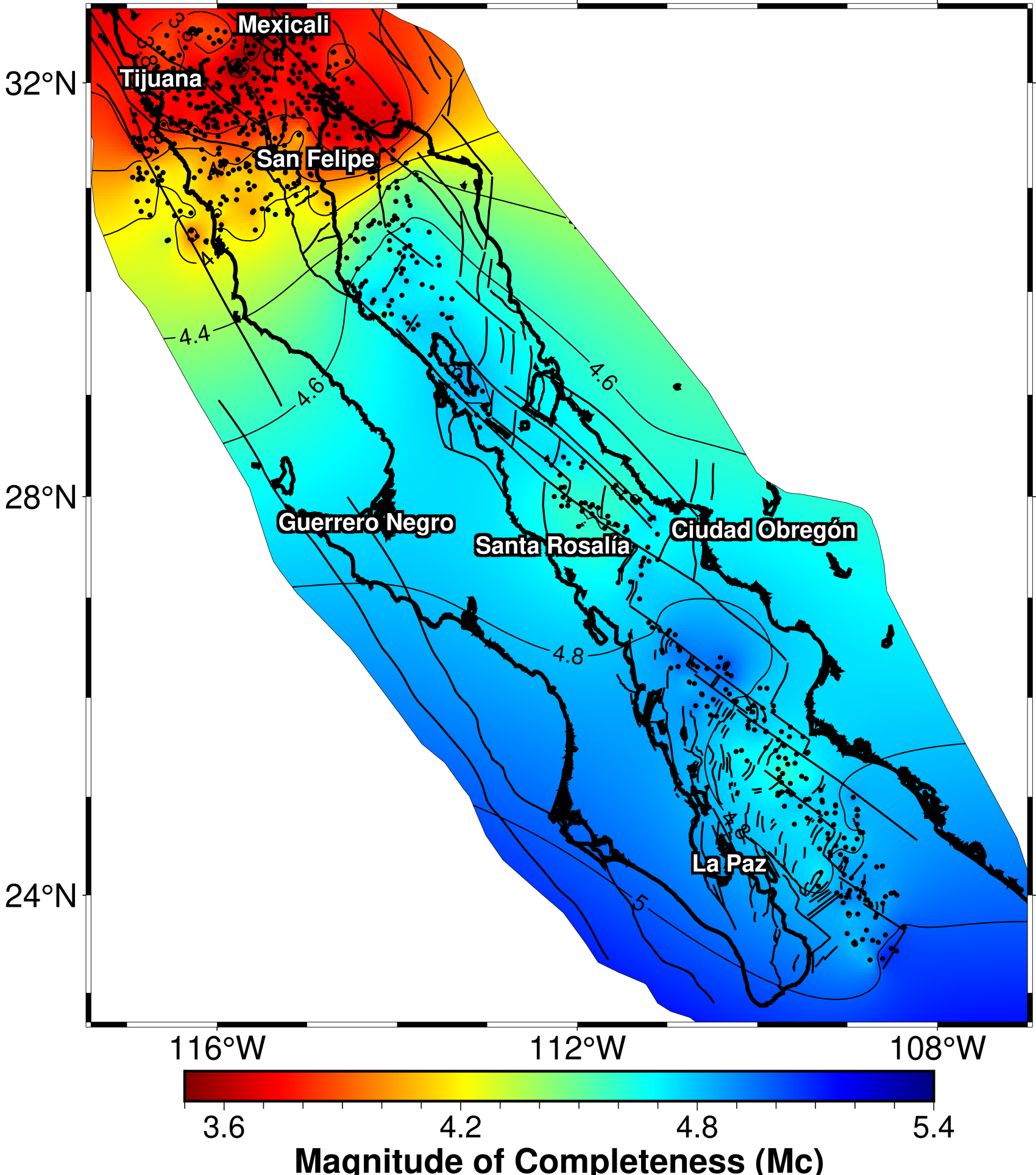
Mexicali
Tijuana
San Felipe
Guerrero Negro
Santa Rosalía
Ciudad Obregón
La Paz
32°N
28°N
24°N
116°W
112°W
108°W
4.4
4.6
4.8
5
3.6
4.2
4.8
5.4
Magnitude of Completeness (Mc)

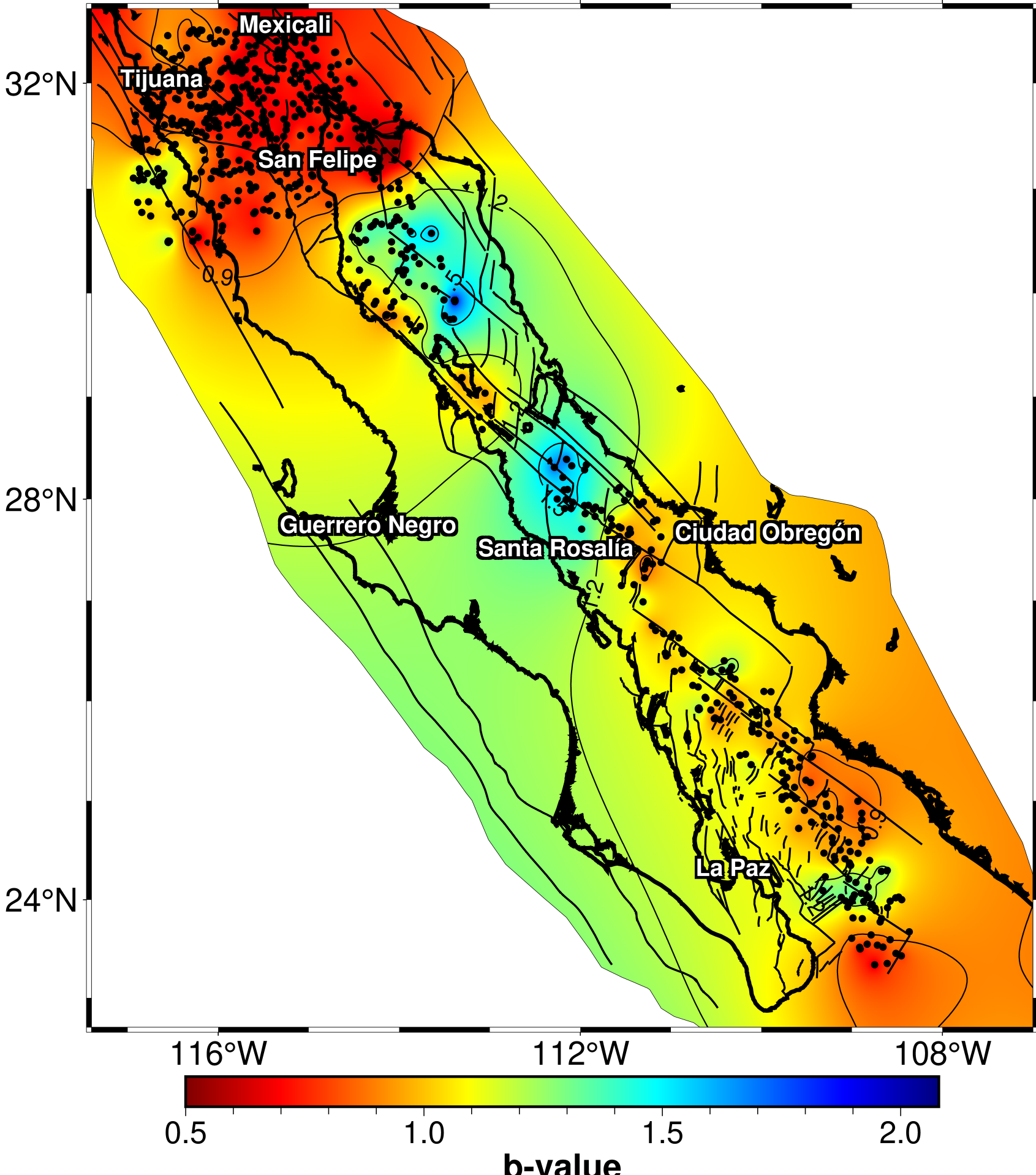

Mexicali
Tijuana
San Felipe
Guerrero Negro
Santa Rosalía
Ciudad Obregón
La Paz
32°N
28°N
24°N
116°W
112°W
108°W
0.5
1.0
1.5
2.0
b-value

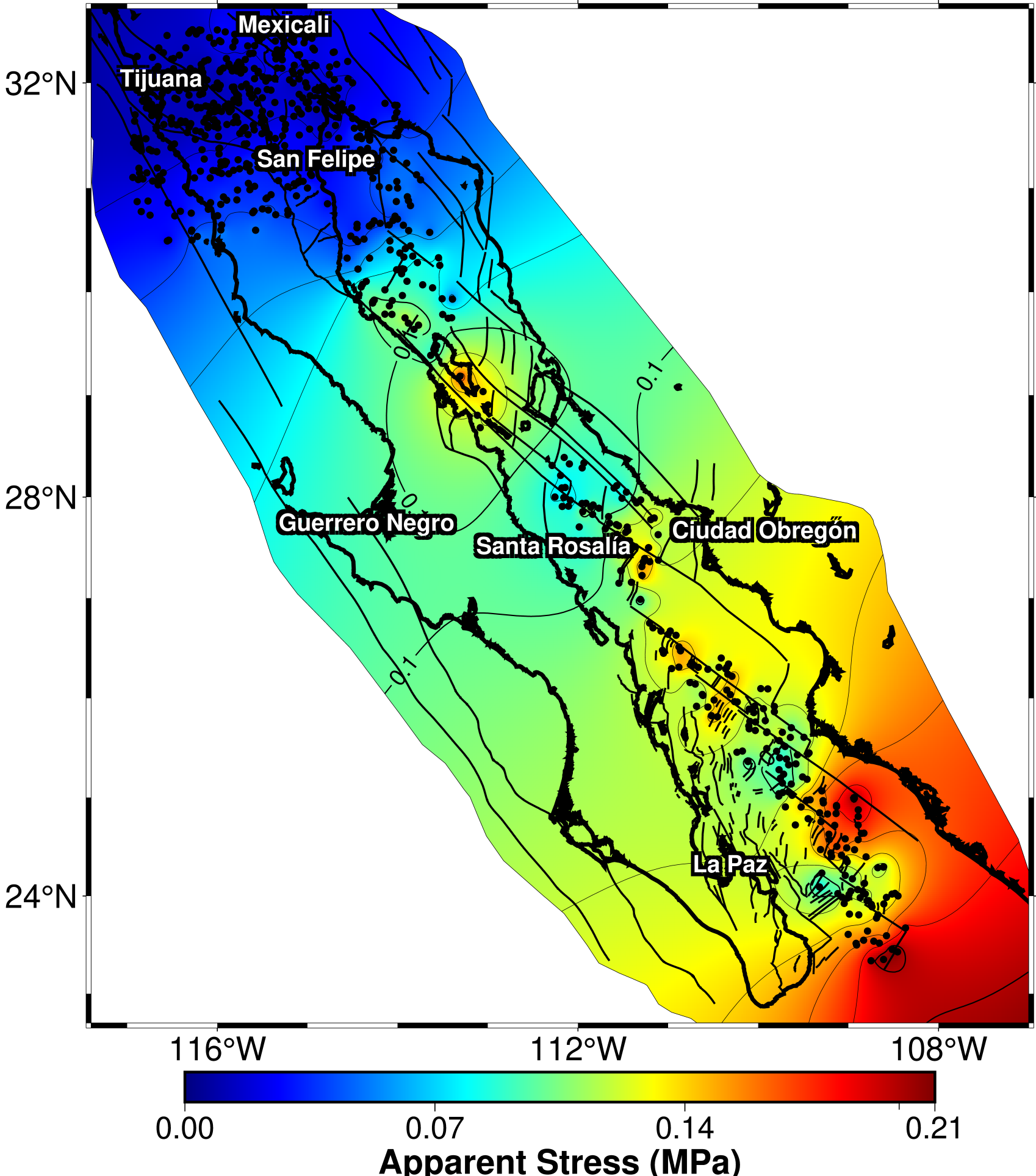
Mexicali
Tijuana
San Felipe
Guerrero Negro
Santa Rosalía
Ciudad Obregón
La Paz
0.1
0
0
0.1
32°N
28°N
24°N
116°W
112°W
108°W
0.00
0.07
0.14
0.21
Apparent Stress (MPa)